AIAA 2002-3861

A Karhunen-Loève Galerkin Technique with Shock Fitting for Optimization of a Blunt Body Geometry

G. P. Brooks and J. M. Powers
Department of Aerospace and
Mechanical Engineering
University of Notre Dame
Notre Dame, Indiana

38th AIAA/ASME/SAE/ASEE Joint Propulsion Conference and Exhibit
7-10 July 2002 / Indianapolis, IN

A KARHUNEN-LOÈVE GALERKIN TECHNIQUE WITH SHOCK FITTING FOR OPTIMIZATION OF A BLUNT BODY GEOMETRY *

Gregory P. Brooks† and Joseph M. Powers‡

Department of Aerospace and Mechanical Engineering,
University of Notre Dame,
Notre Dame, Indiana 46556-5637.

Abstract

A novel Karhunen-Loève (KL) Galerkin model for the supersonic, inviscid flow of a calorically perfect ideal gas about an axisymmetric, blunt body employing shock fitting is developed. The motivation for developing the KL Galerkin model is the need for an accurate and computationally efficient model for use in the optimal design of hypersonic vehicles. In constructing a KL Galerkin model, a set of flow field solutions representative of the design space are required. For this, a global polynomial pseudospectral method for the generalized coordinate, nonconservative form of the Euler equations is implemented. The variables in the equations are collocated via Lagrange interpolating polynomials defined at the zeroes of the Chebyshev polynomials, *i.e.* Chebyshev-Gauss-Lobatto nodes. Code verification, validation and grid convergence results are shown for the pseudospectral code, and an optimal geometry is identified from a single degree of freedom family of geometries. In conclusion the KL modes derived from pseudospectral solutions at Mach 3.5 from a uniform sampling of the design space are presented. This will be used in forthcoming work to develop a KL Galerkin model for the blunt body optimization.

Introduction

Computer-assisted multi-disciplinary design and optimization in the aeronautical engineering community is a promising area of current research. Until recently, the optimization of air vehicles has relied almost exclusively on low fidelity aerodynamic models due to the need for rapid evaluation of aerodynamic design variables such as lift, drag, or heat transfer. Unfortunately, the use of low fidelity models can lead to unacceptable uncertainties in the final optimal design, especially where design safety margins are tight [1]. In addition, low fidelity models often do not provide the complete flow field information such as pressure, temperature, and velocity distributions, acoustic signature, shock wave location, etc. which the designer may be require. For these reasons, high fidelity models such as the Euler or Navier Stokes equations are required. For most problems, these model equations require a discrete solution.

A major difficulty in employing discrete solvers in a multi-disciplinary design process is the large central processing unit (CPU) requirements of these codes. It is not uncommon for discrete solutions to three dimensional flows around complex aircraft configurations to require on the order of ten or more hours of CPU time per steady state solution [1] and these solutions are likely not fully resolved. Complete resolution of complex flow structures could require considerably more CPU time. A design cycle incorporating multiple disciplines, *e.g.* aerodynamics, structures, controls, may easily have hundreds or even thousands of design variables. While interdisciplinary coordination schemes using varying fidelity models [2] help to alleviate the CPU cost associated with interdisciplinary dependence, the aerodynamics discipline alone could still involve a hundred or more design variables. For this reason, current gradient-based numerical optimizers can be prohibitively expensive when used directly with discrete solvers of high fidelity models and approximation becomes necessary.

Review

One popular approximation technique for the de-

 This study has received primary support from the United States Air Force Palace Knight Program and additional support from Los Alamos National Laboratory. Comments by Dr. S. M. Batill are acknowledged.

†Ph.D. Candidate, Student Member AIAA.

‡Associate Professor, Associate Fellow AIAA.

sign of complex, multi-variable problems are response surface approximations [3]. Response surfaces typically approximate quantities such as the lift and drag of the vehicle as a function of the design variables, *e.g.* geometric parameters in terms of simple functional forms. An advantage of the response surface method is that both objective function and gradient evaluation are rapid, on the order of a second or less. Furthermore, polynomial approximation of the objective function ensures that the gradients are continuous. This increases the efficiency of the numerical optimizer in the sense that fewer iterations may be needed to reach an optimum. Two disadvantages of the response surface method are a potential lack of accuracy in capturing the system response by a simple function and also the absence of detailed information about the flow field. Flow field information may be needed for design of a thermal protection system, for coupling with a structural code in static and aeroelastic design, for inverse vehicle design in sonic boom mitigation, acoustic or radar signature reduction, or for shock wave placement for efficient supersonic/hypersonic propulsion.

A recently developed method which does yield detailed flow field information by solution of the governing equations such as the Euler or Navier-Stokes equations is the adjoint method [4–6] taken from control theory [7]. This method is computationally efficient since through the addition of an adjoint equation the governing equations need only be solved once for each iteration of the optimizer regardless of the number of design variables. The adjoint equation is of similar complexity as the governing equations, so each iteration is equivalent in computational cost to two flow field solutions. Although still in development, this method appears to be promising as an accurate and efficient means of multidisciplinary, multi-variable optimal design. Nevertheless, the adjoint method has the disadvantage of requiring that a unique adjoint equation be derived and solved for each new design objective function that may be formulated.

Another approximation technique is the Karhunen-Loève (KL) Galerkin method. This technique is fundamentally a spectral Galerkin method where the basis functions are eigenfunctions of the averaged autocorrelation of previous numerical flow-field solutions. It can be shown that the KL decomposition yields an optimal set of orthonormal basis functions in the sense that the fewest number of functions of all possible bases are required for a given level of accuracy in reconstructing the original set of data. Employing the KL basis functions as the bases of a Galerkin [8], orthogonal collocation [9] or least-squares [10] spectral method, reduced dimension models have been developed which yield accurate solutions to partial differential equations for a computational cost several orders of magnitude lower than discrete solvers. The KL method has advantages over response surfaces in that it generates detailed flow field information and is potentially more accurate. It has advantages over the adjoint method in that the KL model is independent of the design problem formulation. This flexibility in specifying the design problem is an important attribute for an optimal design code [11].

In the present study, a novel KL Galerkin model for the supersonic flow of an inviscid, calorically perfect, ideal gas about an axisymmetric, blunt body using the primitive variable formulation of the unsteady Euler equations in generalized coordinate form is developed. The shock is fitted in order to maintain high accuracy of the model and to avoid the well known Gibbs' phenomena which occurs when trying to capture strong discontinuities using a spectral method [12]. The novelty of the method lies in its use in a compressible flow environment with a moving boundary.

Rusanov [13] as well as Hayes and Probstein [14] have given a thorough review of early contributions to solutions of the supersonic blunt body problem of which a few will be mentioned. Two methodologies for solving the supersonic flow about a blunt body are the direct and inverse methods. The direct method specifies the body shape and then calculates the shock shape and flow field, while the inverse method specifies the shock shape and calculates the body shape which would support that shock shape. At first, studies concerning the inverse problem were founded on series expansion of the governing equations in the vicinity of the shock wave [15]. Later, numerical solutions to the inverse, supersonic blunt body problem were performed by Garabedian and Lieberstein [16] and Van Dyke [17]. Evans and Harlow [18] were the first to generate a numerical solution to the direct problem by integrating the unsteady Euler equations to a relaxed steady state solution using a particle in cell method. Moretti and Abbett [19] used finite differences and fitting of the shock to generate accurate solutions of the Euler equations about a blunt body. Shock-fitted pseudospectral solutions to the Euler equations were first performed by Hussaini, *et al.* [20] and more recently by Kopriva [21].

Outline of KL Method

The first step in generating a KL Galerkin model is generating a set of numerical solutions to the governing equations for a range of design variables. A pseudospectral method is employed for this step. Although there does not appear to be consensus in

the literature for the definition of pseudospectral, we will follow Fornberg [22] and consider a pseudospectral method to be a collocation type of method of weighted residuals, *i.e.* the governing equations are satisfied exactly at collocation points, with the flow quantities represented in terms of global Lagrange interpolating polynomials defined at the collocation points. The spatial derivatives of the flow quantities are then calculated by differentiating the Lagrange interpolating polynomials. Efficient algorithms for calculating derivatives of Lagrange interpolating polynomials on arbitrary grids can be found in Fornberg [22]. The pseudospectral method has two advantages over finite difference or finite volume methods which make it a good candidate for use with the KL method: 1) it is more accurate and 2) integration can be performed by Gaussian quadrature. Accuracy is important since the magnitude of the KL modes decreases rapidly with increasing mode number; two or three orders of magnitude difference are not uncommon between one mode and the next. More modes can be reliably calculated from a pseudospectral method than from finite difference or finite volume methods. In addition, since the solution is known in terms of Lagrange interpolating polynomials, the KL modes can also be expressed in terms of Lagrange polynomials and integration of the KL modes necessary for the Galerkin method can be performed exactly by means of Gaussian quadrature.

The second step in the development of the KL model is to perform a KL decomposition on the characteristic solution set generated by the pseudospectral solver. The KL decomposition, also called Proper Orthogonal Decomposition (POD), appears to have been developed independently in the 1940's by several researchers including Karhunen [23] and Loève [24]. Lumley [25] proposed the KL decomposition as a rational procedure for the extraction of coherent structures in a turbulent flow field. The KL decomposition is also closely related to the singular value decomposition and principal component analysis used in data compression and image processing [27]. As originally introduced by Lumley, the KL decomposition was impractical for more than one spatial dimension. Sirovich [26] introduced the method of snapshots which permitted the KL decomposition to be performed for fully three dimensional flows.

The final step in the development of the KL model is to project the governing equations onto the set of KL modes via a Galerkin method where the boundary conditions are taken into account by integration by parts. Unlike the pseudospectral method, methods such as the spectral Galerkin method represent solutions to the governing equations in terms of a sum of orthogonal functions multiplied by coefficients. The coefficients are calculated by setting the integrated error in the approximation to zero with respect to certain weight functions. The choice of the weight functions determines the type of spectral method. For the spectral Galerkin method, the weight functions are the same orthogonal functions used in approximating the solution. The earliest unified mathematical assessment of the theory of spectral and pseudospectral methods was Gottlieb and Orszag [28]. Significant advances in spectral and pseudospectral methods occurred in the late 1970's and early 1980's and are well documented by Canuto *et al.* [29], with particular application to fluid dynamics. For a more recent review of the application of spectral and pseudospectral methods to hyperbolic problems see Gottlieb and Hesthaven [30].

The KL decomposition has been used in conjunction with the Galerkin method to develop approximate models of turbulent fluid mechanical phenomena, *e.g.* Aubry *et al.* [31], and Sirovich and Park [32,33]. The first use of the KL method for a control application was by Chen and Chang [34], where it was used to control spatiotemporal patterns on a catalytic wafer using experimentally determined KL modes. Independently, Park and Cho [35] developed a KL Galerkin model of the nonlinear heat equation for control or parameter estimation, more recently the KL Galerkin method has been used to solve the Navier-Stokes equations for flow control [36–38] and inverse convection [39–43] and radiation [44] problems. In order to avoid the difficulty of employing the Galerkin method for nonlinear problems, Theodoropulou *et al.* [9] successfully implemented an orthogonal collocation method with numerical KL modes for the optimization of rapid thermal chemical vapor deposition systems in one dimension. LeGresley and Alonso [10] used a KL least-squares model of the Euler equations in a finite volume formulation to optimize the pressure distribution around an airfoil in subsonic flow.

Outline of Paper

In the remainder of this paper, for a model partial differential equation: 1) the Lagrange interpolating polynomial formulation of the pseudospectral method, 2) the KL decomposition, and 3) the KL Galerkin method are presented. Following this, the Euler equations, boundary conditions, geometry of the blunt body, and the single variable blunt body optimization problem are described. Code verification has been performed by comparison to a Taylor-Maccoll solution, but these results will not be presented here. For the blunt body problem, grid convergence tests are presented as well as code validation

results using surface pressure distribution and shock shape. Derivation and implementation of the KL Galerkin model is in progress; results assessing the accuracy and efficiency of the method will be presented in a later paper.

KL Design Optimization Strategy

Step 1: Pseudospectral Solver

The first step in developing a KL model for use in optimization is to generate a set of K characteristic solutions which span the design space of interest in the problem. In the current study, the design space consists of a single geometric variable, b, which parameterizes the problem. The following time dependent partial differential equation in two space dimensions, x and y, gives the solution vector field $\mathbf{U}(x, y, t; b)$ of dimension n,

$$\frac{\partial \mathbf{U}}{\partial t} + \mathbf{A}\frac{\partial \mathbf{U}}{\partial x} + \mathbf{B}\frac{\partial \mathbf{U}}{\partial y} + \mathbf{S} = \mathbf{0}, \tag{1}$$

where $\mathbf{A}$ and $\mathbf{B}$ are flux Jacobian matrices in the x and y directions respectively, and $\mathbf{S}$ is a source term. Although Eq. (1) is time dependent, for the optimal design problem only steady state solutions for various values of b are considered. Solving the time dependent equation to a relaxed steady state is a convenient numerical solution technique. The solution to Eq. (1), $\mathbf{U}(x, y, t; b)$, can be written in terms of a double Lagrange global interpolating polynomial defined on the mesh x_i, $i = 0, ..., N$, y_j, $j = 0, ..., M$, *i.e.*

$$\mathbf{U}(x, y, t; b) = \sum_{i=0}^{N}\sum_{j=0}^{M} \mathbf{U}(x_i, y_j, t; b) L_i^{(N)}(x) L_j^{(M)}(y). \tag{2}$$

The Lagrange interpolating polynomial in the x direction of order N is for example

$$L_i^{(N)}(x) = \frac{\prod_{k=0, k\neq i}^{N} (x - x_k)}{\prod_{k=0, k\neq i}^{N} (x_i - x_k)}, \quad i = 0, ..., N, \tag{3}$$

and a similar expansion defines $L_j^{(M)}(y)$. It is easily shown that the Lagrange interpolating polynomial, $L_i^{(N)}(x)$ has the value of unity at $x = x_i$ and zero at the other collocation points, *i.e.*

$$L_i^{(N)}(x_p) = \delta_{ip} = \begin{cases} 0 & \text{if } i \neq p, \\ 1 & \text{if } i = p. \end{cases}; \tag{4}$$

likewise, $L_j^{(M)}(y)$ is equal to unity at $y = y_j$ and zero at the other collocation points.

Derivatives of $\mathbf{U}(x, y, t; b)$ are evaluated by differentiating Eq. (2). Evaluating these derivatives on the grid, (x_p, y_q), chosen to be the same grid as that used to define the interpolating polynomial, *i.e.* $(x_p, y_q) \equiv (x_i, y_j)$, and making use of Eq. (4) yields

$$\left.\frac{\partial \mathbf{U}}{\partial x}\right|_{(x_p, y_q)} = \sum_{i=0}^{N} \mathbf{U}(x_i, y_q, t; b) \frac{dL_i}{dx}(x_p), \tag{5}$$
$$\left.\frac{\partial \mathbf{U}}{\partial y}\right|_{(x_p, y_q)} = \sum_{j=0}^{M} \mathbf{U}(x_p, y_j, t; b) \frac{dL_j}{dy}(y_q).$$

The terms $\frac{dL_i}{dx}(x_p)$ and $\frac{dL_j}{dy}(y_q)$ in Eq. (5) can be evaluated efficiently for an arbitrary grid using an algorithm developed by Fornberg [22]. The points which both uniquely define the Lagrange interpolating polynomials and at which derivatives are evaluated are the zeroes of Chebyshev polynomials or simply, the Gauss-Lobatto Chebyshev nodes, *i.e.*

$$x_i = \frac{1}{2}\left[1 - \cos\left(\frac{\pi}{N} i\right)\right], \quad i = 0, ..., N, \tag{6}$$
$$y_j = \frac{1}{2}\left[1 - \cos\left(\frac{\pi}{M} j\right)\right], \quad j = 0, ..., M.$$

The Gauss-Lobatto Chebyshev grid is used because global Lagrange polynomial approximations of general nonperiodic functions defined on this grid were found to yield a more uniform and overall lower error than a uniform grid. Substituting the approximations for the derivatives of $\mathbf{U}(x, y, t; b)$ from Eq. (5) into Eq. (1) results in a system of ordinary differential equations (ODEs) in time at the grid points (x_p, y_q), $p = 0, ..., N$, $q = 0, ..., M$. This system of ODEs, *i.e.*

$$\left.\frac{d\mathbf{U}}{dt}\right|_{(x_p, y_q)} = -\mathbf{A}(\mathbf{U})|_{(x_p, y_q)} \sum_{i=0}^{N} \mathbf{U}(x_i, y_q, t; b) \frac{dL_i}{dx}(x_p)$$
$$- \mathbf{B}(\mathbf{U})|_{(x_p, y_q)} \sum_{j=0}^{M} \mathbf{U}(x_p, y_j, t) \frac{dL_j}{dy}(y_q) - \mathbf{S}(\mathbf{U})|_{(x_p, y_q)},$$
$$p = 0, ..., N, \quad q = 0, ..., M, \tag{7}$$

are integrated in time from an arbitrary initial state subject to boundary conditions using a fourth order Runge Kutta technique until a converged steady state is achieved. Equation (7) is solved to steady state for K distinct values of the geometric variable, b_m, $m = 1, ..., K$, yielding K characteristic solutions, $\mathbf{U}_m(x, y)$, $m = 1, ..., K$.

Step 2: Karhunen-Loève Theory

The second step in the development of the KL model is to perform a KL decomposition on the set of

characteristic solutions, $\mathbf{U}_m(x,y)$, $m=1,...,K$, generated in the previous section. We will derive the KL decomposition using a more detailed and transparent process than often is given in the literature.

The motivation behind the KL decomposition is the desire to obtain a series of L orthonormalized functions, $\widehat{\varphi}_i(\mathbf{x})$ such that

$$\int_\Omega \widehat{\varphi}_i(\mathbf{x})\,\widehat{\varphi}_j(\mathbf{x})\,d\mathbf{x} = \delta_{ij}, \quad \begin{matrix} i=1,...,L, \\ L \le K, \end{matrix} \tag{8}$$

where $\mathbf{x}\in\Omega$, and upon approximating the members of an ensemble of functions, $u_m(\mathbf{x})$, $m=1,...,K$, in a finite expansion of the $\widehat{\varphi}_i(\mathbf{x})$, the ensemble average mean-square error, ε^2, is a minimum. Here $\mathbf{x}$ is a spatial variable of dimension two for this problem and $u_m(\mathbf{x})$ is a component of the steady state vector field $\mathbf{U}_m(x,y)$. Mathematically, the coefficients a_{mi} and the set of functions $\widehat{\varphi}_i(\mathbf{x})$ are sought which minimize the following expression:

$$\varepsilon^2 = \frac{1}{K\int_\Omega d\mathbf{x}} \sum_{m=1}^{K} \int_\Omega \left[u_m(\mathbf{x}) - \sum_{i=0}^{L} a_{mi}\widehat{\varphi}_i(\mathbf{x}) \right]^2 d\mathbf{x}. \tag{9}$$

It is here shown that choosing the coefficients, a_{mi}, to be

$$a_{mi} = \int_\Omega u_m(\mathbf{x})\,\widehat{\varphi}_i(\mathbf{x})\,d\mathbf{x}, \quad \begin{matrix} m=1,...,K \\ i=1,...,L \end{matrix}, \tag{10}$$

will minimize ε^2 in Eq. (9). For any other choice of coefficients b_{mi}, ε^2 is

$$\varepsilon^2 = \frac{1}{K\int_\Omega d\mathbf{x}} \sum_{m=1}^{K} \int_\Omega \left[u_m(\mathbf{x}) - \sum_{i=0}^{L} b_{mi}\widehat{\varphi}_i(\mathbf{x}) \right]^2 d\mathbf{x}. \tag{11}$$

Substituting the following expression for the b_{mi},

$$\sum_{i=0}^{L} b_{mi} = \sum_{i=0}^{L} a_{mi} - \sum_{i=0}^{L} (a_{mi} - b_{mi}), \tag{12}$$

into Eq. (11) and making use of Eqs. (8) and (10), ε^2 in Eq. (11) is after simplification,

$$\varepsilon^2 = \frac{1}{K\int_\Omega d\mathbf{x}} \sum_{m=1}^{K} \left(\int_\Omega \left[u_m(\mathbf{x}) - \sum_{i=0}^{L} a_{mi}\widehat{\varphi}_i(\mathbf{x}) \right]^2 d\mathbf{x} + \sum_{i=0}^{L} (a_{mi} - b_{mi})^2 \right), \tag{13}$$

from which it is clear that choosing $b_{mi} = a_{mi}$ minimizes ε^2.

Having found the optimal choice of a_{mi} from Eq. (10), the set of functions, $\widehat{\varphi}_i(\mathbf{x})$, $i=0,...,L$, which minimize ε^2 are found next. Substituting Eq. (10) into Eq. (9) and imposing the restriction of orthonormality from Eq. (8), Eq. (9) becomes:

$$\varepsilon^2 = \frac{1}{K\int_\Omega d\mathbf{x}} \sum_{m=1}^{K} \left(\int_\Omega [u_m(\mathbf{x})]^2 d\mathbf{x} - \sum_{i=0}^{L} \int_\Omega u_m(\mathbf{x})\,\widehat{\varphi}_i(\mathbf{x})\,d\mathbf{x} \int_\Omega u_m(\mathbf{x}')\,\widehat{\varphi}_i(\mathbf{x}')d\mathbf{x}' \right). \tag{14}$$

Observing that the terms $\int_\Omega [u_m(\mathbf{x})]^2 d\mathbf{x}$ and $\int_\Omega d\mathbf{x}$ in Eq. (14) are constants, it is evident that minimizing ε^2 is equivalent to maximizing:

$$\int_\Omega \int_\Omega \mathbf{R}(\mathbf{x},\mathbf{x}') \sum_{i=0}^{L} \widehat{\varphi}_i(\mathbf{x})\widehat{\varphi}_i(\mathbf{x}')d\mathbf{x}d\mathbf{x}', \tag{15}$$

where

$$\mathbf{R}(\mathbf{x},\mathbf{x}') = \frac{1}{K} \sum_{m=1}^{K} u_m(\mathbf{x})u_m(\mathbf{x}'). \tag{16}$$

subject to Eq. (8).

Next the maximization of Eq. (15) from calculus of variations is considered. Suppose that $\varphi_i(\mathbf{x})$, $i=1,...,L$, are the functions which maximize the expression in Eq. (15). Then any functions, $\widehat{\varphi}_i(\mathbf{x})$ can be written as $\widehat{\varphi}_i(\mathbf{x}) = \varphi_i(\mathbf{x}) + \epsilon\varphi_i'(\mathbf{x})$, where ϵ is a constant and $\varphi_i'(\mathbf{x})$ is an arbitrary function. Substituting $\widehat{\varphi}_i(\mathbf{x}) = \varphi_i(\mathbf{x}) + \epsilon\varphi_i'(\mathbf{x})$ into Eq. (15), the function to be maximized $f(\epsilon)$, becomes

$$f(\epsilon) = \int_\Omega \int_\Omega \mathbf{R}(\mathbf{x},\mathbf{x}') \sum_{i=0}^{L} [\varphi_i(\mathbf{x}) + \epsilon\varphi_i'(\mathbf{x})] [\varphi_i(\mathbf{x}') + \epsilon\varphi_i'(\mathbf{x}')]\,d\mathbf{x}d\mathbf{x}', \tag{17}$$

subject to Eq. (8). In order to solve this constrained maximization problem, the method of Lagrange multipliers is employed and a maximum for the following modified function $f^*(\epsilon)$ is sought:

$$f^*(\epsilon) = \int_\Omega \int_\Omega \mathbf{R}(\mathbf{x},\mathbf{x}') \sum_{i=0}^{L} [\varphi_i(\mathbf{x}) + \epsilon\varphi_i'(\mathbf{x})] [\varphi_i(\mathbf{x}') + \epsilon\varphi_i'(\mathbf{x}')]\,d\mathbf{x}d\mathbf{x}' - \sum_{i=0}^{L} \lambda_i \left(\int_\Omega [\varphi_i(\mathbf{x}') + \epsilon\varphi_i'(\mathbf{x}')] [\varphi_i(\mathbf{x}') + \epsilon\varphi_i'(\mathbf{x}')]\,d\mathbf{x}' - 1 \right), \tag{18}$$

where the λ_i are the Lagrange multipliers. Now for a maximum, we it is required that $\frac{d}{d\epsilon} f^*(\epsilon) = 0$ at

$\epsilon = 0$. Differentiating Eq. (18) with respect to ϵ and evaluating at $\epsilon = 0$ yields the following equation after simplifying

$$\begin{aligned}\left.\frac{d}{d\epsilon} f^*(\epsilon)\right|_{\epsilon=0} &= \int_\Omega \int_\Omega \mathbf{R}(\mathbf{x},\mathbf{x}') \sum_{i=0}^{L} [\varphi_i(\mathbf{x})\varphi_i'(\mathbf{x}') \\ &\quad + \varphi_i'(\mathbf{x})\varphi_i(\mathbf{x}') d\mathbf{x} d\mathbf{x}'] \\ &\quad - 2\sum_{i=0}^{L} \lambda_i \int_\Omega \varphi_i(\mathbf{x}')\varphi_i'(\mathbf{x}') d\mathbf{x}' \\ &\quad = 0.\end{aligned} \tag{19}$$

Since, by definition, $\mathbf{R}(\mathbf{x},\mathbf{x}') = \mathbf{R}(\mathbf{x}',\mathbf{x})$ in Eq. (16) and since $\mathbf{x}$ and $\mathbf{x}'$ are dummy variables, it is observed that the two terms involving $\mathbf{R}(\mathbf{x},\mathbf{x}')$ in Eq. (19) are equivalent, so that Eq. (19) can be written as

$$\sum_{i=0}^{L} \int_\Omega \left[\int_\Omega \mathbf{R}(\mathbf{x},\mathbf{x}')\varphi_i(\mathbf{x}) d\mathbf{x} - \lambda_i \varphi_i(\mathbf{x}') \right] \varphi_i'(\mathbf{x}') d\mathbf{x}' = 0. \tag{20}$$

From Eq. (20) it is observed that the quantity in brackets must be equal to zero since the $\varphi_i'(\mathbf{x}')$ are arbitrary, in general non-zero, functions, *i.e.*

$$\int_\Omega \mathbf{R}(\mathbf{x},\mathbf{x}')\varphi_i(\mathbf{x}) d\mathbf{x} = \lambda_i \varphi_i(\mathbf{x}'), \quad i = 0, ..., L. \tag{21}$$

It is recognized that Eq. (21) is simply the definition for the eigensystem for the linear integral operator

$$\int_\Omega \mathbf{R}(\mathbf{x},\mathbf{x}')(\cdot)\, d\mathbf{x}, \tag{22}$$

so that the finite series of orthonormal functions which minimize Eq. (9) are the first L eigenfunctions of this operator. Since the operator in Eq. (22) is symmetric and positive definite, the eigenfunctions, $\varphi_i(\mathbf{x})$, are orthogonal, and the eigenvalues, λ_i, are all real and positive.

Next the computation of the eigensystem in Eq. (21) by the method of snapshots as proposed by Sirovich [26] is considered. Since the operator kernel $\mathbf{R}(\mathbf{x},\mathbf{x}')$ is composed of K linearly independent solutions, $u_m(\mathbf{x})$, $m = 1, ..., K$, the eigenfunctions, $\varphi_i(\mathbf{x})$ can be expressed as a linear combination of these solutions, *i.e.*

$$\varphi_i(\mathbf{x}) = \sum_{j=1}^{K} \alpha_{ij} u_j(\mathbf{x}), \quad i = 1, ..., K. \tag{23}$$

Substituting Eq. (23) into Eq. (21) and making use of Eq. (16) yields

$$\begin{aligned}&\int_\Omega \frac{1}{K} \sum_{m=1}^{K} u_m(\mathbf{x}) u_m(\mathbf{x}') \sum_{j=1}^{K} \alpha_{ij} u_j(\mathbf{x}) d\mathbf{x} \\ &= \lambda_i \sum_{j=1}^{K} \alpha_{ij} u_j(\mathbf{x}'), \quad i = 1, ..., K,\end{aligned} \tag{24}$$

or after simplifying

$$\sum_{m=1}^{K} \alpha_{im} \mathbf{C}_{jm} = \lambda_i \alpha_{ij}, \quad \begin{matrix} i = 1, ..., K, \\ j = 1, ..., K, \end{matrix} \tag{25}$$

where

$$\mathbf{C}_{jm} = \frac{1}{K} \int_\Omega u_j(\mathbf{x}) u_m(\mathbf{x}) d\mathbf{x}. \tag{26}$$

Solving the discrete eigenvalue problem for the α_{ij} from Eq. (25), the eigenvectors of Eq. (22) are then reconstructed via Eq. (23). This procedure will be repeated for each of the n components of the steady state solution vector $\mathbf{U}(x, y; b)$.

Step 3: Galerkin Projection

The final step in developing a KL Galerkin approximation to a partial differential equation is a projection of the differential equation onto the KL modes according to the Galerkin method. The same time dependent partial differential equation as in Eq. (1) with boundary conditions on the domain, $x \in [0,1]$ and $y \in [0,1]$ is taken. The solution to each of the n components of $\mathbf{U}(x,y,t)$, $u^k(x,y,t)$, $k = 1, ..., n$, is approximated by a series expansion in their respective KL modes, $\varphi_j^k(x,y)$, $k = 1, ..., n$, $j = 1, ..., L$, *i.e.*

$$\begin{bmatrix} u^1(x,y,t) \\ u^2(x,y,t) \\ \vdots \\ u^n(x,y,t) \end{bmatrix} \approx \begin{bmatrix} \sum_{j=1}^{L} a_j^1(t)\varphi_j^1(x,y) \\ \sum_{j=1}^{L} a_j^2(t)\varphi_j^2(x,y) \\ \vdots \\ \sum_{j=1}^{L} a_j^n(t)\varphi_j^n(x,y) \end{bmatrix}, \tag{27}$$

where superscripts distinguish the vector components. The right hand side of Eq. (27) is defined as the approximate solution vector, $\mathbf{U}_a(x,y,t)$, and its n components are $u_a^k(x,y,t)$, $k = 1, ..., n$. The coefficients $a_j^k(t)$, $k = 1, ..., n$, $j = 1, ..., L$, are determined as follows. Substituting the approximation $\mathbf{U}_a(x,y,t)$ a residual error for $\mathbf{U}(x,y,t)$ in Eq. (1),

results.

$$\mathbf{e}(x,y,t) = \begin{bmatrix} e^1(x,y,t) \\ e^2(x,y,t) \\ \vdots \\ e^n(x,y,t) \end{bmatrix} = \frac{\partial}{\partial t} \begin{bmatrix} u_a^1(x,y,t) \\ u_a^2(x,y,t) \\ \vdots \\ u_a^n(x,y,t) \end{bmatrix} ($$

$$+ \mathbf{A}\frac{\partial \mathbf{U}_a}{\partial x} + \mathbf{B}\frac{\partial \mathbf{U}_a}{\partial y} + \mathbf{S}$$

It is now enforced that each component of the resic error vector $\mathbf{e}(x,y,t)$, $e^k(x,y,t)$, be orthogona each of the KL modes, $\varphi_j^k(x,y)$, $j = 1,...,L$, t correspond to that component, *i.e.*

$$\begin{bmatrix} \int_0^1 \int_0^1 e^1(x,y,t)\,\varphi_i^1(x,y)\,dxdy \\ \int_0^1 \int_0^1 e^2(x,y,t)\,\varphi_i^2(x,y)\,dxdy \\ \vdots \\ \int_0^1 \int_0^1 e^n(x,y,t)\,\varphi_i^n(x,y)\,dxdy \end{bmatrix} = \begin{bmatrix} 0 \\ 0 \\ \vdots \\ 0 \end{bmatrix} ($$

$i = 1,...,L.$

Substituting both the expression for $\mathbf{e}(x,y,t)$, fi Eq. (28) and $\mathbf{U}_a(x,y,t)$ from Eq. (27) into Eq. (and making use of the orthonormality of the modes, the following KL Galerkin model of Eq. is obtained:

$$\frac{d}{dt}a_i^k(t) = -\int_0^1\int_0^1 \left[\mathbf{A}\frac{\partial \mathbf{U}_a}{\partial x} + \mathbf{B}\frac{\partial \mathbf{U}_a}{\partial y} \right. ($$
$$\left. + \mathbf{S}\right]\varphi_i^k(x,y)\,dxdy,$$
$$k = 1,...,n, \quad i = 1,...,L.$$

The boundary conditions are incorporated i Eq. (30) by performing integration by parts on the tegrals in Eq. (30) and replacing the resulting bou ary terms by the boundary conditions of the probl The integrals in Eq. (30) are evaluated by Gauss-Legendre quadrature.

Supersonic Blunt Body Problem

Governing Equations

Each of the three steps in developing a KL model of the Euler equations for the supersonic flow around a blunt body are now performed. The two-dimensional, axisymmetric, Euler equations for a calorically perfect, ideal gas are, in dimensionless form:

$$\frac{\partial \rho}{\partial t} + u\frac{\partial \rho}{\partial r} + w\frac{\partial \rho}{\partial z} + \rho\left(\frac{\partial u}{\partial r} + \frac{\partial w}{\partial z} + \frac{u}{r}\right) = 0, \quad (31)$$

$$\frac{\partial u}{\partial t} + u\frac{\partial u}{\partial r} + w\frac{\partial u}{\partial z} + \frac{1}{\rho}\frac{\partial p}{\partial r} = 0, \quad (32)$$

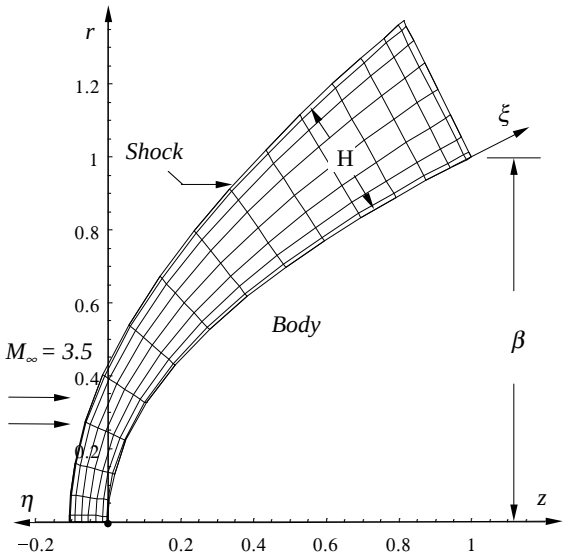

Figure 1: Schematic of shock-fitted high Mach number flow over an axisymmetric blunt body including computational (ξ,η) and physical (r,z) coordinates.

$$\frac{\partial w}{\partial t} + u\frac{\partial w}{\partial r} + w\frac{\partial w}{\partial z} + \frac{1}{\rho}\frac{\partial p}{\partial z} = 0, \quad (33)$$

$$\frac{\partial p}{\partial t} + u\frac{\partial p}{\partial r} + w\frac{\partial p}{\partial z} + \gamma p\left(\frac{\partial u}{\partial r} + \frac{\partial w}{\partial z} + \frac{u}{r}\right) = 0, \quad (34)$$

where ρ is density, p is pressure, u and w are the velocity in the r and z directions respectively, t is time, and γ is the ratio of specific heats. The dimensional form for pressure, p^*, density, ρ^*, and r and z components of velocity, u^* and w^* respectively are recovered by the following equations,

$$p^* = pp_\infty, \quad (35)$$

$$\rho^* = \rho\rho_\infty, \quad (36)$$

$$u^* = u\sqrt{p_\infty/\rho_\infty}, \quad w^* = w\sqrt{p_\infty/\rho_\infty}, \quad (37)$$

where freestream quantities are denoted by ∞. The dimensional space and time variables are

$$z^* = zL, \quad r^* = rL, \quad (38)$$

$$t^* = tL/\sqrt{p_\infty/\rho_\infty}, \quad (39)$$

where L is the length of the body. The body, Fig. 1, is defined by the equation

$$r = \beta z^b, \quad (40)$$

where $\beta = \frac{R}{L}$, is the ratio of the body base radius, R, to its length, L.

To facilitate the solution to the Euler equations for varying geometry, Eqs. $(31-34)$ are rewritten in terms of a general body fitted coordinate system $\xi(z,r,t)$, $\eta(z,r,t)$ and $\tau(z,r,t)$ by making the following substitutions into Eqs. $(31-34)$:

$$\begin{aligned}\frac{\partial}{\partial z} &= \xi_z\frac{\partial}{\partial \xi} + \eta_z\frac{\partial}{\partial \eta} + \tau_z\frac{\partial}{\partial \tau},\\ \frac{\partial}{\partial r} &= \xi_r\frac{\partial}{\partial \xi} + \eta_r\frac{\partial}{\partial \eta} + \tau_r\frac{\partial}{\partial \tau},\\ \frac{\partial}{\partial t} &= \xi_t\frac{\partial}{\partial \xi} + \eta_t\frac{\partial}{\partial \eta} + \tau_t\frac{\partial}{\partial \tau},\end{aligned} \tag{41}$$

where the subscript denotes differentiation with respect to that variable. Finally, taking $\tau(z,r,t) = t$, the nondimensional form of Eqs. $(31-34)$ in generalized coordinates is

$$\frac{\partial \mathbf{U}}{\partial \tau} + \mathbf{A}\frac{\partial \mathbf{U}}{\partial \xi} + \mathbf{B}\frac{\partial \mathbf{U}}{\partial \eta} + \mathbf{S} = \mathbf{0}, \tag{42}$$

where

$$\mathbf{U} = \begin{bmatrix} \rho \\ u \\ w \\ p \end{bmatrix}, \quad \mathbf{S} = \begin{bmatrix} \rho u/r \\ 0 \\ 0 \\ \gamma p u/r \end{bmatrix}, \tag{43}$$

$$\mathbf{A} = \begin{bmatrix} U^c & \rho\xi_r & \rho\xi_z & 0 \\ 0 & U^c & 0 & \xi_r/\rho \\ 0 & 0 & U^c & \xi_z/\rho \\ 0 & \gamma p\xi_r & \gamma p\xi_z & U^c \end{bmatrix}, \tag{44}$$

$$\mathbf{B} = \begin{bmatrix} W^c & \rho\eta_r & \rho\eta_z & 0 \\ 0 & W^c & 0 & \eta_r/\rho \\ 0 & 0 & W^c & \eta_z/\rho \\ 0 & \gamma p\eta_r & \gamma p\eta_z & W^c \end{bmatrix},$$

and

$$\begin{aligned} U^c &= \xi_t + u\xi_r + w\xi_z,\\ W^c &= \eta_t + u\eta_r + w\eta_z. \end{aligned} \tag{45}$$

The grid in the computational domain, Fig. 2, is specified according to a Gauss-Lobatto Chebyshev distribution, *i.e.*,

$$\begin{aligned}\xi_i &= \frac{1}{2}\left(1 - \cos\left(\frac{i}{N}\pi\right)\right) \quad i = 0,1,...,N,\\ \eta_j &= \frac{1}{2}\left(1 - \cos\left(\frac{j}{M}\pi\right)\right) \quad j = 0,1,...,M,\end{aligned} \tag{46}$$

where $N+1$ are the number of nodes in the ξ direction and $M+1$ are the number in the η direction.

The physical grid in Fig. 1 is constructed such that the grid is normal to both the boundary at $r = 0$, and the body.

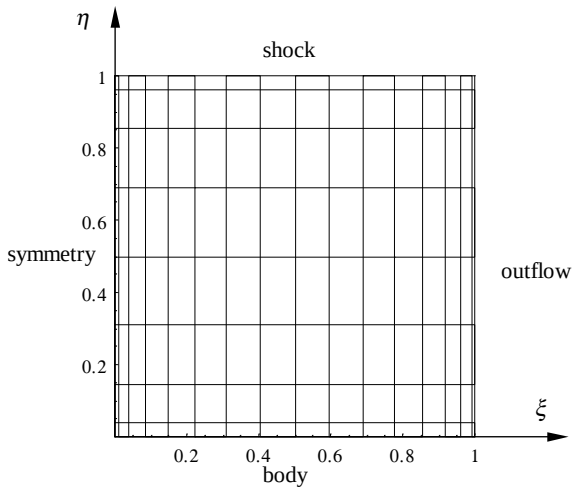

Figure 2: Gauss-Lobatto Chebyshev computational grid for the shock-fitted blunt body.

Boundary Conditions

The kinematic boundary condition at the body is that the normal velocity component be equal to zero, *i.e.*

$$\mathbf{v}\cdot\mathbf{e}_\eta|_{\eta=0} = 0, \tag{47}$$

where $\mathbf{v}$ is the velocity vector, *i.e.*

$$\mathbf{v} = u\mathbf{e}_r + w\mathbf{e}_z,$$

and $\mathbf{e}_\eta$ is the body normal vector, *i.e.*

$$\mathbf{e}_\eta = \frac{\xi_z\mathbf{e}_r - \xi_r\mathbf{e}_z}{\sqrt{\xi_z^2 + \xi_r^2}}, \tag{48}$$

expressed in terms of the unit vectors $\mathbf{e}_r$ and $\mathbf{e}_z$, in the r and z directions respectively. From the fact that at the body, $\mathbf{e}_\eta$ is normal to the unit vector in the ξ direction, $\mathbf{e}_\xi$, *i.e.* $(\mathbf{e}_\eta\cdot\mathbf{e}_\xi)|_{\eta=0} = 0$, where

$$\mathbf{e}_\xi = \frac{-\eta_z\mathbf{e}_r + \eta_r\mathbf{e}_z}{\sqrt{\eta_z^2 + \eta_r^2}}, \tag{49}$$

it is found that

$$\mathbf{e}_\eta|_{\eta=0} = \frac{-\eta_r\mathbf{e}_r - \eta_z\mathbf{e}_z}{\sqrt{\eta_z^2 + \eta_r^2}}, \tag{50}$$

so that Eq. (47) becomes

$$\mathbf{v}\cdot\mathbf{e}_\eta|_{\eta=0} = -(u\eta_r + w\eta_z)|_{\eta=0} = -W^c|_{\eta=0} = 0. \tag{51}$$

In order to formulate a stable numerical boundary condition at the body for ρ, u, w, and p,

Eq. (42) is rewritten in the following characteristic formulation [45,46]:

$$\mathbf{R}\frac{\partial \mathbf{U}}{\partial \tau} + \mathbf{R}\mathbf{A}\frac{\partial \mathbf{U}}{\partial \xi} + \mathbf{\Lambda}_\eta \mathbf{R}\frac{\partial \mathbf{U}}{\partial \eta} + \mathbf{R}\mathbf{S} = \mathbf{0}. \tag{52}$$

The square matrix, $\mathbf{R}$, in Eq. (52) contains the left eigenvectors of $\mathbf{B}$ in its rows. The diagonal matrix $\mathbf{\Lambda}_\eta$ contain the eigenvalues of $\mathbf{B}$ in its diagonal. The diagonal eigenvalue matrix, $\mathbf{\Lambda}_\eta$, and the left eigenvector matrix $\mathbf{R}$ are:

$$\mathbf{\Lambda}_\eta = \begin{bmatrix} W^c & 0 & 0 & 0 \\ 0 & W^c & 0 & 0 \\ 0 & 0 & W^{c-} & 0 \\ 0 & 0 & 0 & W^{c+} \end{bmatrix}, \tag{53}$$

$$\mathbf{R} = \begin{bmatrix} 0 & -\frac{\eta_z\eta_r}{\eta_z^2+\eta_r^2} & \frac{\eta_z^2}{\eta_z^2+\eta_r^2} & 0 \\ 1 & 0 & 0 & -\frac{1}{c^2} \\ 0 & -\frac{\rho c \eta_z}{2\sqrt{\eta_z^2+\eta_r^2}} & -\frac{\rho c \eta_r}{2\sqrt{\eta_z^2+\eta_r^2}} & \frac{1}{2} \\ 0 & \frac{\rho c \eta_z}{2\sqrt{\eta_z^2+\eta_r^2}} & \frac{\rho c \eta_r}{2\sqrt{\eta_z^2+\eta_r^2}} & \frac{1}{2} \end{bmatrix}, \tag{54}$$

where $c = \sqrt{\gamma p/\rho}$ is the dimensionless acoustic speed and $W^{c\pm} = W^c \pm c\sqrt{\eta_z^2+\eta_r^2}$. Only the first three of the equations in Eq. (52) can be used as numerical boundary conditions since they are associated with negative eigenvalues, $\mathbf{\Lambda}_\eta$. The fourth equation in Eq. (52) is associated with a positive eigenvalue and thus describes information propagation from inside the body which must therefore be discarded as non-physical; in its place the physical boundary condition, $\mathbf{v}\cdot\mathbf{e}_\eta|_{\eta=0}$, is solved. Substituting the restrictions that, $\mathbf{v}\cdot\mathbf{e}_\eta|_{\eta=0} = W^c = 0$, and $\frac{\partial W^c}{\partial \tau} = 0$, into the first three equations in Eq. (52) yields

$$\eta_z\frac{\partial(u)}{\partial\tau} - \eta_r\frac{\partial(w)}{\partial\tau} = U^c\left(\eta_r\frac{\partial w}{\partial\xi} - \eta_z\frac{\partial u}{\partial\xi}\right) + \frac{1}{\rho}\left(\eta_r\xi_z - \eta_z\xi_r\right)\frac{\partial p}{\partial\xi}, \tag{55}$$

$$\frac{\partial\rho}{\partial\tau} = \frac{1}{c^2}\frac{\partial p}{\partial\tau} - U^c\left(\frac{\partial\rho}{\partial\xi} - \frac{1}{c^2}\frac{\partial p}{\partial\xi}\right), \tag{56}$$

$$\begin{aligned}\frac{\partial p}{\partial\tau} = {} & c\sqrt{\eta_z^2+\eta_r^2}\frac{\partial p}{\partial\eta} + \frac{\rho c U^c}{\sqrt{\eta_z^2+\eta_r^2}}\left(\eta_r\frac{\partial u}{\partial\xi}\right. \\ & \left.+\eta_z\frac{\partial w}{\partial\xi} + \frac{(\eta_r\xi_r+\eta_z\xi_z)}{\rho U^c}\frac{\partial p}{\partial\xi}\right) - U^c\frac{\partial p}{\partial\xi} \\ & - \rho c^2\left(\xi_r\frac{\partial u}{\partial\xi} + \xi_z\frac{\partial w}{\partial\xi} + \eta_r\frac{\partial u}{\partial\eta} + \eta_z\frac{\partial w}{\partial\eta}\right) \\ & - \frac{\rho c^2 u}{r}.\end{aligned} \tag{57}$$

At the shock boundary, the Rankine-Hugoniot relations are solved along with a compatibility equation. Specifically, the Rankine-Hugoniot relations are:

$$\mathbf{v}_1\cdot\mathbf{e}_T = \mathbf{v}_2\cdot\mathbf{e}_T, \tag{58}$$

$$\delta_2 = \frac{\gamma-1}{\gamma+1}\delta_1 + \frac{2\gamma}{\gamma+1}\frac{p_1}{\rho_1\delta_1}, \tag{59}$$

$$p_2 = \frac{2}{\gamma+1}\rho_1\delta_1^2 - \frac{\gamma-1}{\gamma+1}p_1, \tag{60}$$

$$\frac{\rho_2}{\rho_1} = \frac{\delta_1}{\delta_2}, \tag{61}$$

where

$$\begin{aligned}\delta_i &= \mathbf{v}_i\cdot\mathbf{e}_N - \widetilde{v}, \\ &= \mathbf{v}_i\cdot\mathbf{e}_N - (\mathbf{e}_\eta\cdot\mathbf{e}_N)\,v.\end{aligned} \tag{62}$$

In Eqs. $(58-62)$, $\mathbf{e}_T$ and $\mathbf{e}_N$ are unit vectors in the shock tangential and normal directions respectively, and $\widetilde{v}$ and v are the velocity of the shock in the, $\mathbf{e}_N$, and, $\mathbf{e}_\eta$, directions respectively. Quantities denoted with a subscript of 1 are freestream quantities and those with subscript 2 are on the downstream side of the shock. The unit vectors $\mathbf{e}_T$ and $\mathbf{e}_N$, are in terms of the inverse metrics

$$\begin{aligned}\mathbf{e}_T &= \frac{-\eta_z\mathbf{e}_r + \eta_r\mathbf{e}_z}{\sqrt{\eta_z^2+\eta_r^2}}, \\ \mathbf{e}_N &= \frac{\eta_r\mathbf{e}_r + \eta_z\mathbf{e}_z}{\sqrt{\eta_z^2+\eta_r^2}}.\end{aligned} \tag{63}$$

In order to solve the Rankine-Hugoniot equations, an expression for the shock velocity in the body normal direction, v, is needed. Differentiating Eqs. (59) and (60) with respect to time in the body normal coordinate system (ξ,η,τ), yields

$$\begin{aligned}\frac{\partial\delta_2}{\partial\tau} &= A\frac{\partial\delta_1}{\partial\tau} + B\frac{\partial p_1}{\partial\tau} + C\frac{\partial\rho_1}{\partial\tau}, \\ \frac{\partial p_2}{\partial\tau} &= D\frac{\partial\delta_1}{\partial\tau} + E\frac{\partial p_1}{\partial\tau} + F\frac{\partial\rho_1}{\partial\tau}\end{aligned} \tag{64}$$

where

$$\begin{aligned}&A = \frac{\gamma-1}{\gamma+1} - \frac{2\gamma}{\gamma+1}\frac{p_1}{\rho_1\delta_1^2}, \quad B = \frac{2\gamma}{(\gamma+1)\,\rho_1\delta_1}, \\ &C = -B\frac{p_1}{\rho_1}, \quad D = \frac{4\rho_1\delta_1}{\gamma+1}, \\ &E = -\frac{\gamma-1}{\gamma+1}, \quad F = \frac{2\delta_1^2}{\gamma+1}.\end{aligned} \tag{65}$$

Since the freestream flow is steady, it is found that

$$\begin{aligned}\frac{\partial\delta_2}{\partial\tau} &= A\frac{\partial\delta_1}{\partial\tau}, \\ \frac{\partial p_2}{\partial\tau} &= D\frac{\partial\delta_1}{\partial\tau},\end{aligned} \tag{66}$$

where from Eq. (62) it is seen that

$$\frac{\partial \delta_i}{\partial \tau} = \frac{\partial \mathbf{v}_i}{\partial \tau} \cdot \mathbf{e}_N + \mathbf{v}_i \cdot \frac{\partial \mathbf{e}_N}{\partial \tau} - (\mathbf{e}_\eta \cdot \mathbf{e}_N) \frac{\partial v}{\partial \tau} - v \mathbf{e}_\eta \cdot \frac{\partial \mathbf{e}_N}{\partial \tau}. \quad (67)$$

By substituting Eq. (67) into Eq. (66), then multiplying the first equation in (66) by $\rho_2 c_2$ and adding it to the second equation in (66), the shock acceleration $\frac{\partial v}{\partial \tau}$,

$$\frac{\partial v}{\partial \tau} = \frac{1}{(\mathbf{e}_\eta \cdot \mathbf{e}_N)\left[D + \rho_2 c_2 (A-1)\right]} \left[\frac{\partial \mathbf{e}_N}{\partial \tau} \cdot \left[(D + \rho_2 c_2 A)(\mathbf{v}_1 - v\mathbf{e}_\eta) - \rho_2 c_2 (\mathbf{v}_2 - v\mathbf{e}_\eta) \right] - \rho_2 c_2 \frac{\partial \mathbf{v}_2}{\partial \tau} \cdot \mathbf{e}_N - \frac{\partial p_2}{\partial \tau} \right], \quad (68)$$

is found. The terms $\frac{\partial p_2}{\partial \tau}$ and $\rho c \frac{\partial \mathbf{v}_2}{\partial \tau} \cdot \mathbf{e}_N$ must be specified by a compatibility equation which is the characteristic equation associated with the wave propagating from the interior to the back of the shock along the normal direction. This compatibility equation is in the same form as the fourth compatibility equation in Eq. (52) only written in shock coordinates instead of the body coordinate system (ξ, η, τ). After some simplification the following shock acceleration equation is obtained

$$\frac{\partial v}{\partial \tau} = \frac{(D + \rho_2 c_2 A)(\mathbf{v}_1 - v\mathbf{e}_\eta) \cdot \frac{\partial \mathbf{e}_N}{\partial \tau}}{(\mathbf{e}_\eta \cdot \mathbf{e}_N)\left[D + \rho_2 c_2 (A-1)\right]} - \frac{\rho_2 c_2 (\mathbf{v}_2 - v\mathbf{e}_\eta) \cdot \frac{\partial \mathbf{e}_N}{\partial \tau} + R|_{\eta=1}}{(\mathbf{e}_\eta \cdot \mathbf{e}_N)\left[D + \rho_2 c_2 (A-1)\right]}, \quad (69)$$

where

$$R = U^c \frac{\partial p}{\partial \xi} + W^c \frac{\partial p}{\partial \eta} + \frac{\rho c}{\sqrt{z_\xi^2 + r_\xi^2}} \left[z_\xi \left(U^c \frac{\partial u_r}{\partial \xi} + W^c \frac{\partial u}{\partial \eta} + \frac{1}{\rho} \left(\xi_r \frac{\partial p}{\partial \xi} + \eta_r \frac{\partial p}{\partial \eta} \right) \right) - r_\xi \left(U^c \frac{\partial w}{\partial \xi} + W^c \frac{\partial w}{\partial \eta} + \frac{1}{\rho} \left(\xi_z \frac{\partial p}{\partial \xi} + \eta_z \frac{\partial p}{\partial \eta} \right) \right) \right] + \gamma p \left(\xi_z \frac{\partial w}{\partial \xi} + \eta_z \frac{\partial w}{\partial \eta} + \xi_r \frac{\partial u}{\partial \xi} + \eta_r \frac{\partial u}{\partial \eta} \right) + \frac{\gamma p u}{r}. \quad (70)$$

The time derivative of the normal unit vector is

$$\frac{\partial \mathbf{e}_N}{\partial \tau} = \left(r_\xi \frac{\partial z_\xi}{\partial \tau} - z_\xi \frac{\partial r_\xi}{\partial \tau} \right) \frac{(z_\xi \mathbf{e}_z + r_\xi \mathbf{e}_r)}{\left(z_\xi^2 + r_\xi^2\right)^{3/2}}. \quad (71)$$

The shock distance, H, along the body normal can be found by integrating the following equation,

$$\frac{\partial H}{\partial \tau} = v. \quad (72)$$

The boundary conditions at $\xi = 0$ in computational coordinates are

$$\left.\frac{\partial w}{\partial \xi}\right|_{\xi=0} = 0, \quad \left.\frac{\partial p}{\partial \xi}\right|_{\xi=0} = 0, \quad u|_{\xi=0} = 0, \quad s|_{\xi=0} = s_o. \quad (73)$$

where s is the entropy and s_o is the value of the entropy just behind the shock at $r = 0$. In arriving at Eq. (73), use has been made of the orthogonality of the grid at $r = 0$, *i.e.* $\eta_r|_{r=0} = 0$. The first three boundary conditions in Eq. (73) come from enforcing symmetry of the solution. The boundary condition for entropy comes from casting the energy equation, Eq. (34), in steady-state in terms of the entropy, *i.e.*

$$u \frac{\partial s}{\partial r} + w \frac{\partial s}{\partial z} = 0, \quad (74)$$

and enforcement of $u|_{\xi=0} = 0$ which yields $\left.\frac{\partial s}{\partial z}\right|_{\xi=0} = 0$. Thus $s|_{\xi=0}$ is constant and equal to s_o, the value behind the shock at $\xi = 0$. The density at $\xi = 0$ can subsequently be found by the following equation relating density, pressure and entropy for a calorically perfect, ideal gas,

$$\rho = \left(\frac{p}{s}\right)^{1/\gamma}. \quad (75)$$

At the supersonic outflow boundary, $\xi = 1$, no physical boundary conditions are required, *i.e.* all waves are exiting the domain. Here the governing equations are solved in the same manner as in the interior.

Optimal Design Problem

To illustrate the KL method for an optimal design problem, the power law body in Eq. (40) is considered and the value of b which minimizes the drag coefficient, C_D, over the forebody section only, for fixed freestream Mach number, $M_\infty = 3.5$, ratio of specific heats, $\gamma = \frac{7}{5}$, and aspect ratio $\beta = 1$ is sought. For the axisymmetric problem in dimensionless variables, the equation for $C_D(b)$ is

$$C_D(b) = \frac{4}{\gamma M_\infty^2} \int_0^1 \left[p|_{\eta=0} - 1 \right] r \frac{\partial r}{\partial \xi} d\xi, \quad (76)$$

where $p|_{\eta=0}$ is the nondimensional pressure on the body surface. The integral in Eq. (76) is evaluated by using Gauss-Legendre quadrature.

Spatial Discretization via Lagrange Polynomials

The solution vector, $\mathbf{U}(\xi,\eta,\tau)$ is approximated in terms of a double Lagrange global interpolating polynomial,

$$\mathbf{U}(\xi,\eta,\tau) \approx \sum_{i=0}^{N}\sum_{j=0}^{M} \mathbf{U}(\xi_i,\eta_j,\tau) L_i^{(N)}(\xi) L_j^{(M)}(\eta). \tag{77}$$

The derivatives of $\mathbf{U}(\xi,\eta,\tau)$ with respect to ξ at ξ_p and η at η_q are then

$$\left.\frac{\partial \mathbf{U}}{\partial \xi}\right|_{(\xi_p,\eta_q)} \approx \sum_{i=0}^{N} \mathbf{U}(\xi_i,\eta_q,\tau)\frac{dL_i}{d\xi}(\xi_p), \tag{78}$$
$$\left.\frac{\partial \mathbf{U}}{\partial \eta}\right|_{(\xi_p,\eta_q)} \approx \sum_{j=0}^{M} \mathbf{U}(\xi_p,\eta_j,\tau)\frac{dL_j}{d\eta}(\eta_q).$$

The Chebyshev grid is used to uniquely define the Lagrange interpolating polynomial, *i.e.*

$$\xi_i = \frac{1}{2}\left[1-\cos\left(\frac{\pi}{N}i\right)\right], \quad i=0,...,N, \tag{79}$$
$$\eta_j = \frac{1}{2}\left[1-\cos\left(\frac{\pi}{M}j\right)\right], \quad j=0,...,M.$$

The physical coordinates as a function of the computational coordinates are also approximated by a global Lagrange interpolating polynomial at the Chebyshev points (ξ_i,η_j):

$$z(\xi,\eta,\tau) \approx \sum_{i=0}^{N}\sum_{j=0}^{M} z(\xi_i,\eta_j,\tau) L_i(\xi) L_j(\eta), \tag{80}$$

$$r(\xi,\eta,\tau) \approx \sum_{i=0}^{N}\sum_{j=0}^{M} r(\xi_i,\eta_j,\tau) L_i(\xi) L_j(\eta).$$

The metrics z_ξ, z_η, z_τ, r_ξ, r_η, and r_τ are then found by differentiating Eq. (80). Since the inverse metrics ξ_z, ξ_r, ξ_t, η_z, η_r, and η_t are needed to solve the governing equations, boundary conditions, and shock velocity equation, the following relation between the metrics and inverse metrics

$$\begin{aligned} \xi_z &= \frac{1}{J} r_\eta, & \eta_z &= -\frac{1}{J} r_\xi, \\ \xi_r &= -\frac{1}{J} z_\eta, & \eta_r &= \frac{1}{J} z_\xi, \\ \xi_t &= \frac{(r_\tau z_\eta - r_\eta z_\tau)}{J}, & \eta_t &= \frac{(r_\xi z_\tau - r_\tau z_\xi)}{J}, \\ J &= r_\eta z_\xi - r_\xi z_\eta, \end{aligned} \tag{81}$$

is employed. The metrics $\frac{\partial z_\xi(\xi_p,\eta_{qj},\tau)}{\partial\tau}$ and $\frac{\partial r_\xi(\xi_p,\eta_q,\tau)}{\partial\tau}$ in Eq. (71) are specified by differentiating Eq. (80),

$$\frac{\partial z_\xi(\xi_p,\eta_q,\tau)}{\partial\tau} = \sum_{i=0}^{N}\frac{\partial}{\partial\tau} z(\xi_i,\eta_q,\tau)\frac{dL_i}{d\xi}(\xi_p), \tag{82}$$
$$\frac{\partial r_\xi(\xi_p,\eta_q,\tau)}{\partial\tau} = \sum_{i=0}^{N}\frac{\partial}{\partial\tau} r(\xi_i,\eta_q,\tau)\frac{dL_i}{d\xi}(\xi_p).$$

The terms $\frac{\partial}{\partial\tau} z(\xi_i,\eta_q,\tau)$ and $\frac{\partial}{\partial\tau} r(\xi_i,\eta_q,\tau)$ can be expressed in terms of the shock velocity v, and $\mathbf{e}_\eta$, *i.e.*

$$\begin{aligned} &\frac{\partial}{\partial\tau} z(\xi_i,\eta_q,\tau) \\ &= -\left(1-\cos\left(\frac{q}{M}\pi\right)\right)\left[\frac{\xi_r v\,(\xi_i)}{\sqrt{\xi_z^2+\xi_r^2}}\right]_{\xi_i,\eta_q}, \\ &\frac{\partial}{\partial\tau} r(\xi_i,\eta_q,\tau) \\ &= \left(1-\cos\left(\frac{j}{M}\pi\right)\right)\left[\frac{\xi_z v\,(\xi_i)}{\sqrt{\xi_z^2+\xi_r^2}}\right]_{\xi_i,\eta_q}. \end{aligned} \tag{83}$$

Time Integration

Once the Euler equations (42), the body boundary compatibility equations $(55-57)$, the shock acceleration equation (69), and the shock velocity equation (72) have been discretized using a Lagrange interpolating polynomial approximation, a set of ordinary differential equations of the following form remains

$$\left.\frac{d\mathbf{U}}{d\tau}\right|_{p,q} = -\left[\mathbf{A}\frac{\partial\mathbf{U}}{\partial\xi} + \mathbf{B}\frac{\partial\mathbf{U}}{\partial\eta} + \mathbf{S}\right]_{(\xi_p,\eta_q)}, \tag{84}$$
$$p=0,...,N,$$
$$q=0,...,M.$$

The additional algebraic equations, namely, the Rankine-Hugoniot relations, Eqs. $(58-61)$, the zero normal velocity at the body, Eq. (51), and the discretized form of the symmetry boundary condition, Eq. (73), are needed to completely determine Eq. (84). Eq. (84) is solved using a fourth order Runge-Kutta method with the time step, $\Delta\tau$, corresponding to a CFL number of roughly 0.3, so as to resolve the fastest acoustic time scales. The initial conditions are chosen such that the values for density, pressure, and velocity are constant in the domain and equal to the post shock values with the exception that at the body, the velocity is forced also to satisfy $\mathbf{v}\cdot\mathbf{e}_\eta = 0$. The initial shock shape is chosen such that the distance H is constant and v is initially zero.

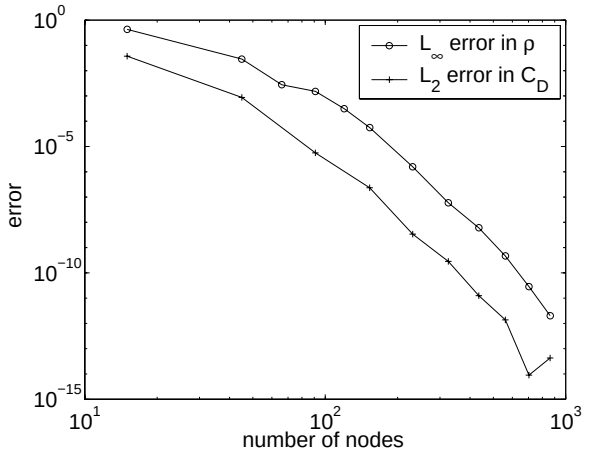

Figure 3: Grid convergence $L_\infty[\Omega]$ error in $\rho(\xi,\eta)$, and L_2 error in C_D measured against a baseline, 65×33 grid, Chebyshev solution for a $b = 0.5$, Mach 3.5 blunt body.

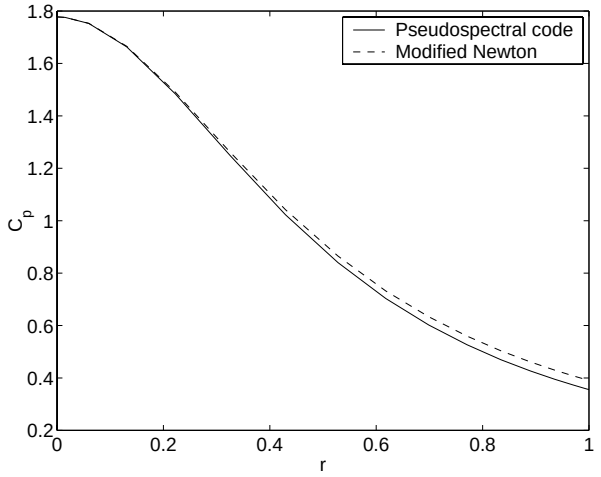

Figure 4: Blunt body surface C_p distribution predictions at Mach 3.5 for modified Newtonian theory and the current code, where $b = 0.5$.

Results

Flow Solver Verification and Validation

A grid convergence study is performed for the blunt body with both the $L_\infty[\Omega]$ error over the domain, $\{\Omega : \xi \in [0,1], \eta \in [0,1]\}$ in $\rho(\xi,\eta)$ and the L_2 error in C_D shown in Fig. 3, where the error is measured against a 65×33 or 2145 node numerical solution. For 703 nodes, the error in C_D has been reduced to the order of 10^{-14} and subsequently flattens due to roundoff error. The maximum local error is approximately two orders of magnitude greater than the error in C_D for every grid resolution.

As a means of code validation, a comparison is made between the numerical results for the pressure distribution on the body with that of the modified Newtonian [47] sine squared law. The modified Newtonian approximation is a semi-empirical model for the surface pressure distribution over blunt bodies. It has been reported by Anderson[48], that for a power law body with $b = 0.5$ and aspect ratio near unity, the modified Newtonian approximation does well in predicting the pressure distribution on the surface of the body. As can be seen from Fig. 4, the pseudospectral code also predicts close agreement for the pressure distribution on the surface of the body defined by $r = \sqrt{z}$. As a further check on the validity of the pseudospectral code, in Fig. 5 a comparison is made of the current prediction for the shock shape for Mach 3.5 flow over a sphere with that of an empirical formula by Billig[49] developed for flow over spherically blunted cones based on experiment. Contour plots of

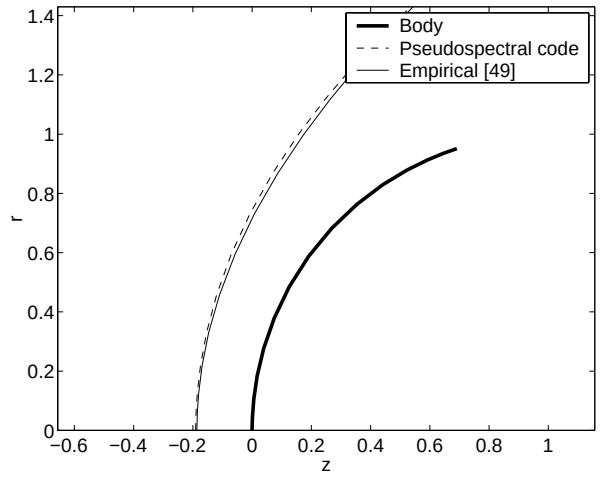

Figure 5: Current method shock shape prediction for a sphere at Mach 3.5 compared with an empirical formula [49] derived from experiments.

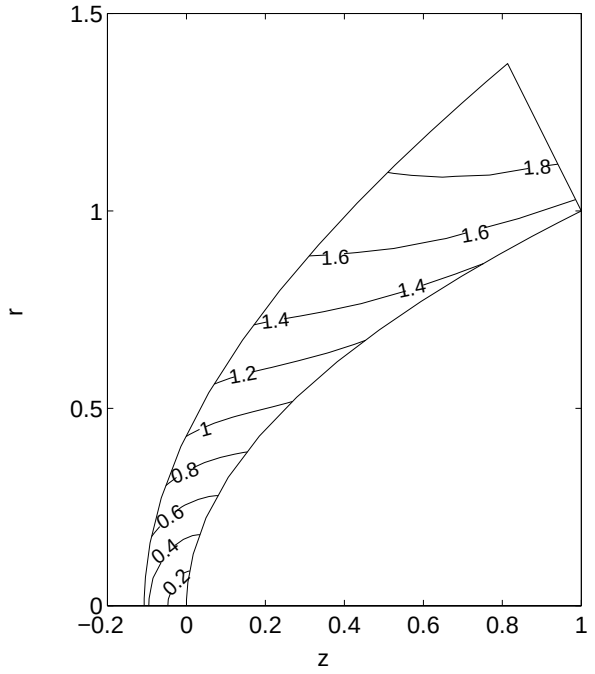

Figure 6: Contour plot of Mach number for Mach 3.5 flow over the blunt body for $b = 0.5$.

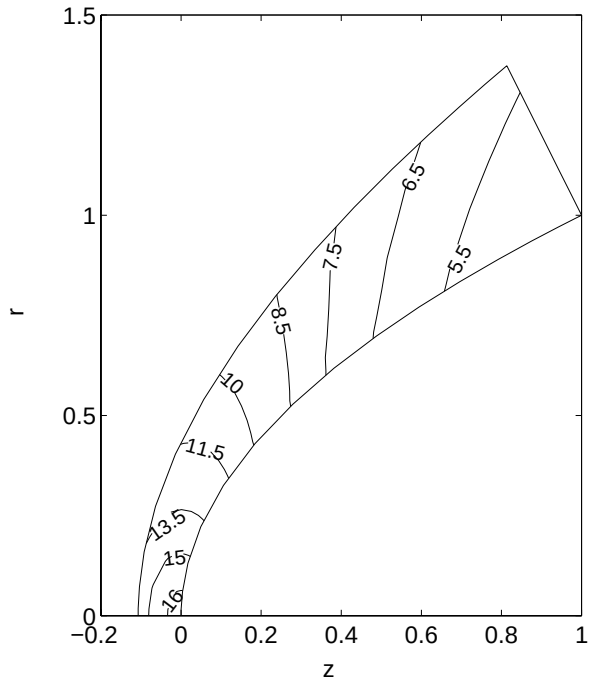

Figure 7: Contour plot of pressure for Mach 3.5 flow over the blunt body for $b = 0.5$.

Mach number and entropy are shown in Figs. 6 and 7.

Finally, a profile of C_D as a function of the power b at Mach 3.5 calculated from the pseudospectral code on a 17×9 grid is shown in Fig. 8. The minimum C_D occurs at approximately $b = 0.35$. The result for the minimum C_D computed in this fashion will be used to compare with the KL method results to be performed in future work.

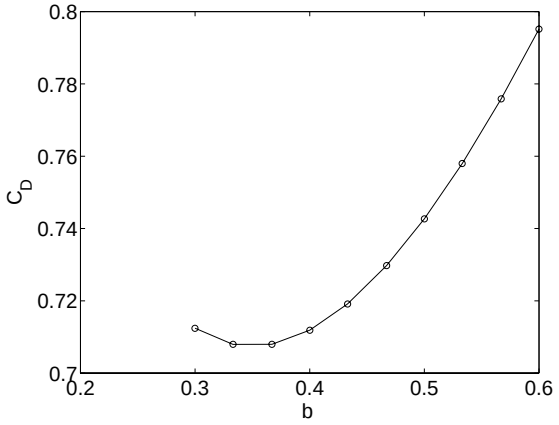

Figure 8: C_D vs. b from a 17×9 grid numerical solution at Mach 3.5.

Blunt Body KL Modes

Ten snapshots are generated for ten different values of b chosen uniformly in the range $0.3 \leq b \leq 0.6$. From these ten snapshots, ten KL modes and associated eigenvalues are calculated for each of the primitive variables: $\{\varphi_n^\rho, \lambda_n^\rho\}$, $\{\varphi_n^u, \lambda_n^u\}$, $\{\varphi_n^w, \lambda_n^w\}$, $\{\varphi_n^p, \lambda_n^p\}$, $n = 1, ..., 10$, where superscripts dictate to which primitive variable the KL modes and eigenvalues are associated. The method of snapshots, Eqs. (25) and (23), was used to generate the KL modes and eigenvalues. A plot of the eigenvalues for density are shown in Fig. 9 while the ten eigenmodes are shown in Fig. 10. There is a rapid decay in the magnitude of the eigenvalues and a progressively more complex set of eigenmodes as the eigenvalue decreases.

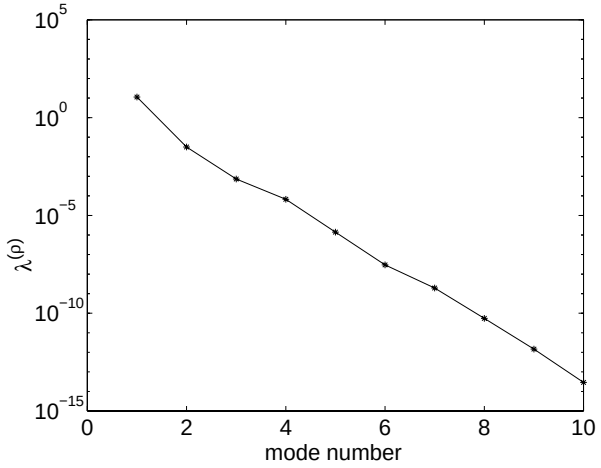

Figure 9: Eigenvalues of density for ten snapshots over the range $0.3 \leq b \leq 0.6$.

Discussion

In this study, a KL Galerkin model of the Euler equations for supersonic flow over a blunt body was developed. It is believed that this is the first study where the KL Galerkin method has been applied to a supersonic problem with shock fitting. In addition, this work is novel in employing the KL Galerkin method for a complex geometry with a complicated moving boundary. Results assessing the accuracy and efficiency of the KL Galerkin model will be presented in a later paper.

Accuracy and efficiency results for the KL Galerkin method from other researchers [36–43] are encouraging; nevertheless, it is still in the early stages of development and much work needs to be done. There are still issues that need to be addressed for applying the KL method to general complex geometries, particularly how to implement the KL method on unstructured or multi-domain structured grids. There are also issues of the necessary number and location of design space samples needed to guarantee a prescribed level of accuracy in the KL Galerkin model. In addition, work is needed in applying the KL method to design problems with a large number of design variables. It has not yet been determined if the cost reduction per KL Galerkin solution will be enough to permit the solution to a large, multi-variable design problem. For large, multi-variable design, it may be necessary to employ various fidelity models such as discrete solvers and response surfaces in a coordinated fashion [2] with the KL Galerkin method.

It is noted that the necessity to use shock fitting to obtain these results is a significant complication that renders application of the KL method to be difficult for problems with embedded discontinuities. It is also noted that for design optimization of vehicles in the hypersonic regime it is more appropriate to employ a viscous model which accounts for real gas effects such as vibrational relaxation and dissociation. In the high Mach number regime in the outer atmosphere, the viscous shock and boundary layer merge and a KL model would no longer require special measures of shock fitting and the KL method of design optimization may be more straightforward.

References

[1] Gnoffo, P. A., Weilmuenster, J. K., Hamilton, H. H., Olynick, D. R., and Venkatapathy, E., "Computational Aerothermodynamic Design Issues for Hypersonic Vehicles," *Journal of Spacecraft and Rockets*, Vol. 36, No. 1, 1999, pp. 21-43.

[2] Rodriguez, J. F., Renaud, J. E., Wujek, B. A., and Tappeta, R. V., "Trust Region Model Management in Multidisciplinary Design Optimization," *Journal of Computational and Applied Mathematics*, Vol. 124, 2000, pp. 139-154.

[3] Batill, S. M., and Stelmack, M. A.,"Framework for Multidisciplinary Design Based on Response-Surface Approximations," *Journal of Aircraft*, Vol. 36, No. 1, 1999, pp. 287-297.

[4] Jameson, A., "Re-Engineering the Design Process Through Computation" *Journal of Aircraft*, Vol. 36, No. 1, 1999, pp. 36-50.

[5] Reuther, J., Alonso, J. J., Rimlinger, M. J., and Jameson, A.,"Aerodynamic Shape Optimization of Supersonic Aircraft Configurations Via an Adjoint Formulation on Distributed Memory Parallel Computers," *Computers and Fluids*, Vol. 28, 1999, pp. 675-700.

[6] Reuther, J. J., Jameson, A., Alonso, J. J., Rimlinger, M. J., and Saunders, D.,"Constrained Multipoint Aerodynamic Shape Optimization Using an Adjoint Formulation and Parallel Computers, Parts 1-2," *Journal of Aircraft*, Vol. 36, No. 1, 1999, pp. 51-74.

[7] Lion, J. L., *Optimal Control of Systems Governed by Partial Differential Equations*, Springer-Verlag, Berlin, 1971.

[8] Park, H. M., and Lee, M. W., "An Efficient Method of Solving the Navier-Stokes Equations for

Flow Control," *International Journal for Numerical Methods in Engineering*, Vol. 41, 1998, pp. 1133-1151.

[9] Theodoropoulou, A., Adomaitis, R. A., and Zafiriou, E., "Model Reduction for Optimization of Rapid Thermal Chemical Deposition Systems," *IEEE Transactions on Semiconductor Manufacturing*, Vol. 11, No. 1, 1998, pp. 85-98.

[10] LeGresley, P. A., and Alonso, J. J., "Airfoil Design Optimization Using Reduced Order Models Based on Proper Orthogonal Decomposition," AIAA Paper 2000-2545, 2000.

[11] Jou, W. H., Huffman, W. P., Young, D. P., Melvin, R. G., Bieterman, M. B., Hilmes, C. L., and Johnson, F. T., "Practical Considerations in Aerodynamic Design Optimization," AIAA Paper 95-1730-CP, 1995.

[12] Hussaini, M. Y., Kopriva, D. A., Salas, M. D., and Zang, T. A. "Spectral Methods for the Euler Equations: Part I-Fourier Methods and Shock Capturing," *AIAA Journal,* Vol. 23, No. 1, 1985, pp. 64-70.

[13] Rusanov, V. V., "A Blunt Body in a Supersonic Stream," *Annual Review of Fluid Mechanics*, Vol. 8, 1976, pp. 377-404.

[14] Hayes, W. D., and Probstein, R. F., *Hypersonic Flow Theory, Vol. 1 Inviscid Flows*, Academic Press, New York, 1966.

[15] Lin, C. C., and Rubinov, S. I., "On the Flow Behind Curved Shocks," *Journal of Mathematics and Physics*, Vol. 27, 1948, pp. 105-129.

[16] Garabedian, P. R., and Lieberstein, H. M., "On the Numerical Calculation of Detached Bow Shock Waves in Hypersonic Flow," *Journal of the Aeronautical Sciences*, Vol. 25, No. 1, 1958, pp. 109-118.

[17] Van Dyke, M. D., "The Supersonic Blunt-Body Problem - Review and Extension," *Journal of the Aero/Space Sciences*, Vol. 25, No. 4, 1958, pp. 485-496.

[18] Evans, M. W., and Harlow, F. H., "Calculation of Supersonic Flow Past an Axially Symmetric Cylinder," *Journal of the Aeronautical Sciences*, Vol. 25, No. 1, 1958, pp. 269-270.

[19] Moretti, G., and Abbett, M., "A Time-Dependent Computational Method for Blunt Body Flows," *AIAA Journal*, Vol. 4, No. 12, 1966, pp. 2136-2141.

[20] Hussaini, M. Y., Kopriva, D. A., Salas, M. D., and Zang, T. A., "Spectral Methods for the Euler Equations: Part 2. Chebyshev Methods and Shock-Fitting," *AIAA Journal*, Vol. 23, No. 2, 1985, pp. 234-240.

[21] Kopriva, D. A., "Shock-fitted Multidomain Solution of Supersonic Flows," *Computer Methods in Applied Mechanics and Engineering,* Vol. 175, 1999, pp. 383-394.

[22] Fornberg, B., *A Practical Guide to Psuedospectral Methods*, Cambridge University Press, Cambridge, 1998.

[23] Karhunen, K., "Zur spektraltheorie stochastischer prozesse," *Annales Academiae Scientiarum Fennicae*, Vol. 34, 1946.

[24] Loève, M., *Probability Theory*, Van Nostrand, Princeton, N.J., 1955.

[25] Lumley, J., *Stochastic Tools in Turbulence*, Academic Press, New York, 1970.

[26] Sirovich, L., "Turbulence and the Dynamics of Coherent Structures. Part 1-3," *Quarterly of Applied Mathematics*, Vol. 45, No. 3, 1987, pp. 561-590.

[27] Rosenfeld, A., and Kak, A. C., *Digital Picture Processing*, Academic Press, New York, 1976.

[28] Gottlieb, D., and Orszag, S., *Numerical Analysis of Spectral Methods: Theory and Applications*, SIAM-CBMS, Philadelphia, 1977.

[29] Canuto, C., Hussaini, M. Y., Quarteroni, A., and Zang, T. A., *Spectral Methods in Fluid Dynamics*, Springer-Verlag, New York, 1988.

[30] Gottlieb, D. and Hesthaven, J. S., "Spectral Methods for Hyperbolic Problems," *Journal of Computational and Applied Mathematics*, Vol. 128, 2001, pp. 83-131.

[31] Aubry, N., Holmes, P., Lumley, J. L., and Stone, E., "The Dynamics of Coherent Structures in the Wall Region of a Turbulent Boundary Layer," *Journal of Fluid Mechanics*, Vol. 192, 1988, pp. 115-173.

[32] Sirovich, L., and Park, H., "Turbulent Thermal Convection in a Finite Domain: Part I. Theory," *Physics of Fluids A*, Vol. 2, No. 9, 1990, pp. 1649-1658.

[33] Park, H., and Sirovich, L., "Turbulent Thermal Convection in a Finite Domain: Part II. Numerical Results," *Physics of Fluids A*, Vol. 2, No. 9, 1990, pp. 1659-1668.

[34] Chen, C.-C., and Chang, H.-C. "Accelerated Disturbance Damping of an Unknown Distributed System by Nonlinear Feedback," *AIChE Journal*, Vol. 38, No. 9, 1992, pp. 1461-1476.

[35] Park, H. M., and Cho, D. H., "The Use of the Karhunen Loève Decomposition for the Modeling of Distributed Parameter Systems," *Chemical Engineering Science*, Vol. 51, No. 1, 1996, pp. 81-98.

[36] Park, H. M., and Lee, M. W., "An Efficient Method of Solving the Navier-Stokes Equations for Flow Control," *International Journal for Numerical Methods in Engineering*, Vol. 41, 1998, pp. 1133-1155.

[37] Park, H. M., and Lee, M. W., "Boundary Control of the Navier-Stokes Equation by Empirical Reduction of Modes," *Computer Methods in Applied Mechanics and Engineering*, Vol. 188, 2000, pp. 165-186.

[38] Park, H. M., and Lee, M. W., "Control of Navier-Stokes Equations by Means of Mode Reduction," *International Journal for Numerical Methods in Fluids*, Vol. 33, 2000, pp. 535-557.

[39] Park, H. M., and Lee, J. H., "A Method of Solving Inverse Convection Problems by Means of Mode Reduction," *Chemical Engineering Science*, Vol. 53, No. 9, 1998, pp. 1731-1744.

[40] Park, H. M., and Lee, J. H., "Reduction of Modes for the Solution of Inverse Natural Convection Problems," *Computer Methods in Applied Mechanics and Engineering*, Vol. 190, 2000, pp. 919-940.

[41] Park, H. M., and Lee, J. H., "Solution of an Inverse Heat Transfer Problem by Means of Empirical Reduction of Modes," *Zeitschrift für angewandte Mathematik und Physik*, Vol. 51, 2000, pp. 17-38.

[42] Park, H. M., and Jung, W. S., "Recursive Solution of an Inverse Heat Transfer Problem in Rapid Thermal Processing Systems," *International Journal of Heat and Mass Transfer*, Vol. 44, 2001, pp. 2053-2065.

[43] Park, H. M., and Jung, W. S., "The Karhunen-Loève Galerkin Method for the Inverse Natural Convection Problems," *International Journal of Heat and Mass Transfer*, Vol. 44, 2001, pp. 155-167.

[44] Park, H. M., and Yoon, T. Y., "Solution of Inverse Radiation Problems Using the Karhunen-Loève Galerkin Procedure," *Journal of Quantitative Spectroscopy & Radiative Transfer*, Vol. 68, 2001, pp. 489-506.

[45] Thompson, K. W., "Time Dependent Boundary Conditions for Hyperbolic Systems," *Journal of Computational Physics*, Vol. 68, 1987, pp. 1-24.

[46] Thompson, K. W., "Time Dependent Boundary Conditions for Hyperbolic Systems, II," *Journal of Computational Physics*, Vol. 89, 1990, pp. 439-461.

[47] Lees, L., "Hypersonic Flow," *Proceedings of the Fifth International Aeronautical Conference, Los Angeles*, Institute of the Aeronautical Sciences, New York, 1955, pp. 241-275.

[48] Anderson, J. D., *Hypersonic and High Temperature Gas Dynamics*, McGraw-Hill, New York, 1989.

[49] Billig, F. S., "Shock-wave Shapes Around Spherical and Cylinder-nosed Bodies," *Journal of Spacecraft and Rockets*, Vol. 4, No. 6, 1967, pp. 822-823.

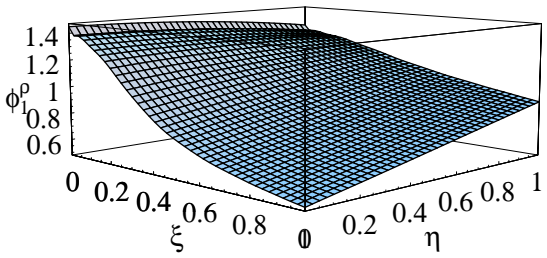

(a) $\lambda_1^\rho = 11.29$

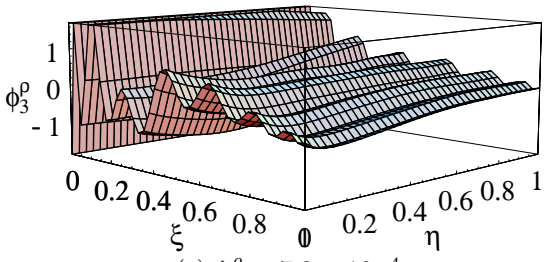

(c) $\lambda_3^\rho = 7.3 \times 10^{-4}$

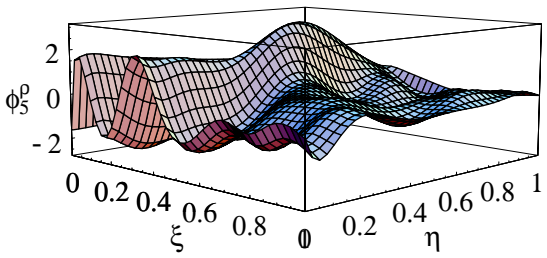

(e) $\lambda_5^\rho = 1.4 \times 10^{-6}$

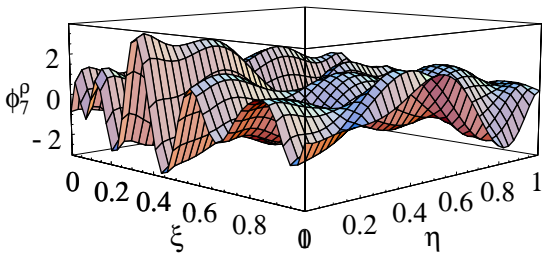

(g) $\lambda_7^\rho = 1.94 \times 10^{-9}$

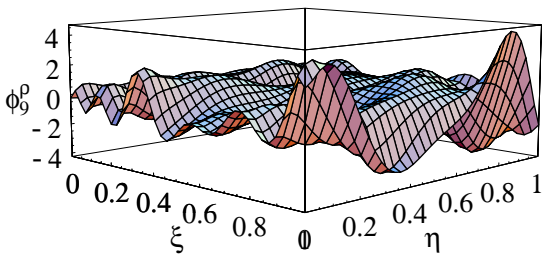

(i) $\lambda_9^\rho = 1.47 \times 10^{-12}$

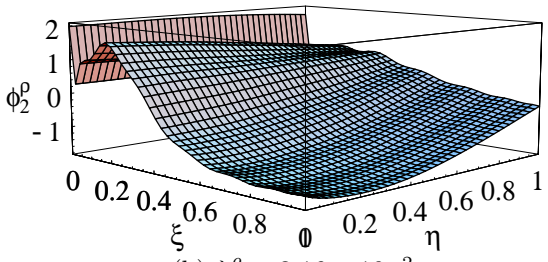

(b) $\lambda_2^\rho = 3.16 \times 10^{-2}$

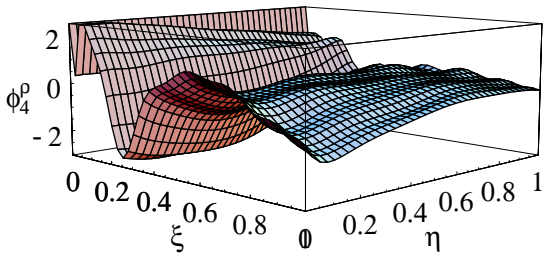

(d) $\lambda_4^\rho = 6.68 \times 10^{-5}$

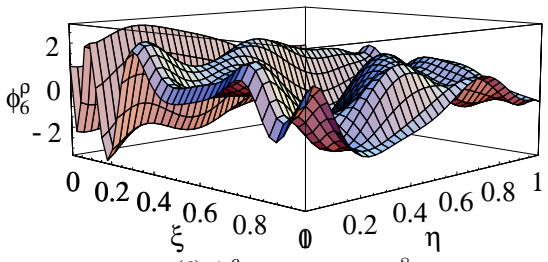

(f) $\lambda_6^\rho = 2.95 \times 10^{-8}$

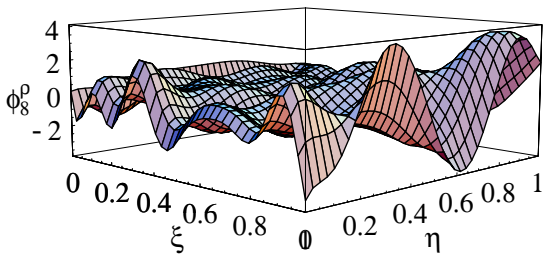

(h) $\lambda_8^\rho = 5.45 \times 10^{-11}$

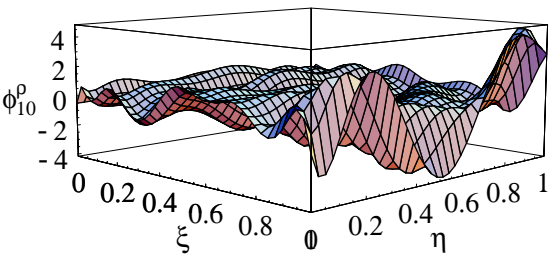

(j) $\lambda_{10}^\rho = 2.9 \times 10^{-14}$

Figure 10: Ten KL eigenmodes of density with associated eigenvalues, λ_n^ρ.